Comparison of Autler–Townes splitting based absolute measurements of the $^7Li_2$ $A\ ^1\Sigma_u^+ - X\ ^1\Sigma_g^+$ electronic transition dipole moment with *ab initio* theory

O. Salihoglu,[1] P. Qi,[1] E. H. Ahmed,[1] S. Kotochigova,[1] S. Magnier,[2] and A. M. Lyyra[1,a)]
[1]*Physics Department, Temple University, Philadelphia, Pennsylvania 19122-6082, USA*
[2]*Institut de Physique de Rennes (UMR UR1-CNRS 6251), Université Rennes I, Bât. 11B, Campus de Beaulieu, F-35042 Rennes Cedex, France*

(Received 15 July 2008; accepted 24 September 2008; published online 3 November 2008)

We report a comparison between experimental and theoretical electronic transition dipole moment values for the $^7Li_2$ $A\ ^1\Sigma_u^+ - X\ ^1\Sigma_g^+$ system. The experimental results are based on measuring the absolute magnitude of the transition dipole matrix elements from Autler–Townes splitting of rovibrational transitions for different *R*-centroid values. The *ab initio* theoretical calculations of the transition dipole moment for the $^7Li_2$ $A\ ^1\Sigma_u^+ - X\ ^1\Sigma_g^+$ system were performed using two different quantum-mechanical models: an all-electron valence bond self-consistent-field method and a pseudopotential molecular orbital method. As expected for the smallest molecule with core electrons, the agreement between experiment and theory is very good. © *2008 American Institute of Physics*. [DOI: 10.1063/1.3000416]

I. INTRODUCTION

Investigations of coherence and quantum interference effects in atomic and molecular systems have led to the discovery of a number of interesting phenomena such as electromagnetically induced transparency (EIT),[1–4] coherent population trapping,[5–7] ultraslow propagation of light,[8,9] and Autler–Townes (AT) splitting.[10–13] The original groundbreaking work on EIT by Imamoglu and Harris[14] was first reported in an atomic system[15] and followed by studies of various excitation configurations.[16]

Molecular systems offer opportunities for a rich variety of excitation schemes, but present also serious challenges. They are much more complex in terms of their energy level structure and relaxation mechanisms than atomic systems. Each molecular electronic state consists of a large number of rovibrational levels. Because an excited state rovibronic level is coupled to rovibronic energy levels in other electronic states by spontaneous decay and other relaxation mechanisms, the system is unavoidably open. In contrast to the open system, a system is considered closed if the excitation and decay processes do not involve energy levels beyond those that are needed for the observation of the coherence effect. In this sense atoms are examples of closed systems.

Molecular transitions have smaller transition dipole moments and as a result the available Rabi frequencies are much smaller than in atomic cases. Furthermore, due to their dense energy level structure high spectral resolution is required in such experiments, which further complicates the situation, since the required continuous wave (cw) lasers have weaker electric field amplitudes further aggravating the situation with poor Rabi frequencies $\Omega = \mu E/\hbar$, where μ is the electronic transition dipole moment matrix element and E is the coupling laser electric field amplitude. An additional difficulty is also the need to overcome the residual Doppler broadening[17] in thermal molecular samples. As a result, research on quantum interference effects in molecular systems has been reported only more recently. These reports have produced some surprising differences compared to closed atomic systems.

To overcome the difficulties with the weaker oscillator strengths of molecular transitions, the first observation of the AT effect in a molecular system was demonstrated in H_2 by Quesada *et al.*[18] in a pulsed laser experiment. However, more recently it was discovered that a judicious choice of laser wavelengths and beam propagation geometry can help overcome the Doppler effect[19–21] in cw laser experiments. Such a molecular cascade excitation system experiment was used to demonstrate the measurement of the absolute magnitude of the transition dipole moment matrix element between two excited states[22] and for characterization of radiative properties of highly excited molecular states.[23] In addition, we have observed that the molecular lambda scheme exhibits a robust EIT pattern and the vee scheme exhibits EIT even in the counterpropagating configuration,[24] a result that is counterintuitive in view of the fact that the residual Doppler width is less favorable in this case[17] compared to the copropagating laser arrangement. This surprising result is a manifestation of the open nature of molecular systems.[24]

To avoid multiphoton ionization of pulsed laser excitation, higher order multiple resonance excitation schemes have provided a powerful tool to overcome the Doppler broadening of the thermal molecular sample. For example, excitation schemes involving more than three independently tunable lasers that are based on triple or quadruple resonance spectroscopic techniques[25–27] have the advantage that the first laser excitation facilitates the selection of a narrow ve-

a)Electronic mail: lyyra@temple.edu.

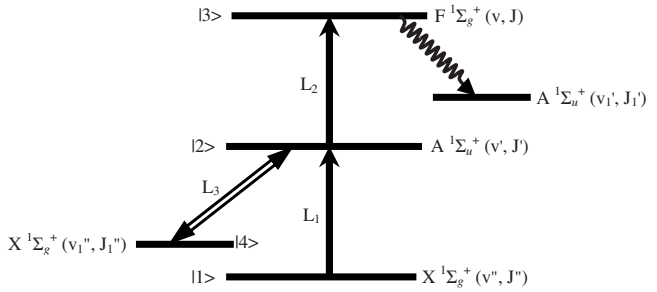

FIG. 1. Li_2 Energy level diagram for the extended Λ four-level system. The pump (L_1) and coupling (L_3) lasers excite molecules from lower states $X\ ^1\Sigma_g^+(v'',J'')$ and $X\ ^1\Sigma_g^+(v_1'',J_1'')$ (|1⟩ and |4⟩), respectively, to the same intermediate state $A\ ^1\Sigma_u^+(v',J')$ (|2⟩). The AT splitting spectra are observed by monitoring fluorescence of a given rovibronic transition $F\ ^1\Sigma_g^+(v,J) \rightarrow A\ ^1\Sigma_u^+(v_1',J_1')$ as a function of the probe laser L_2 detuning around the resonance frequency of the transition between the upper state $F\ ^1\Sigma_g^+(v,J)$ (|3⟩) state and the intermediate state $A\ ^1\Sigma_u^+(v',J')$ (|2⟩), which is also the upper level of the coupling laser transition. Such a probe laser scan reveals the AT splitting of the intermediate level |2⟩ when the probe laser Rabi frequency is small compared to the coupling laser Rabi frequency.

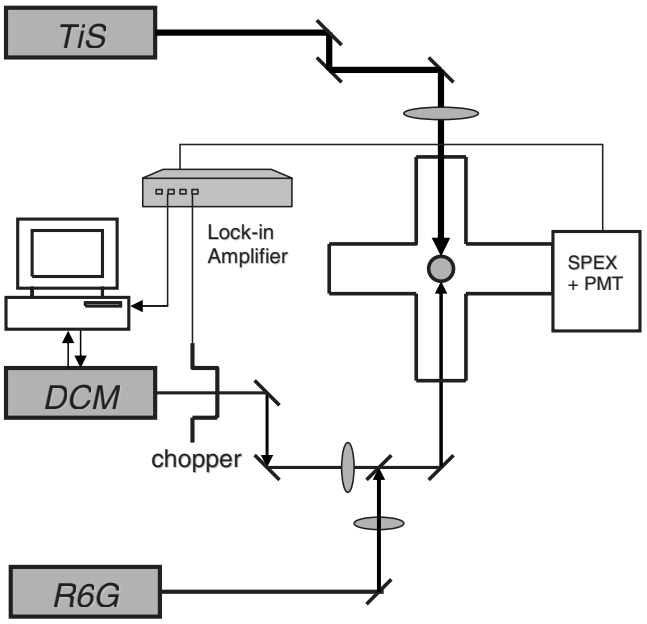

FIG. 2. Experimental setup: The four-level (extended Λ-configuration) excitation scheme was used with the two dye laser beams (DCM and R6G) copropagating in the opposite direction of the coupling field (TiS). A mechanical chopper was used to modulate one of the dye laser beams for phase-sensitive detection. The resulting double resonance signal was detected by a SPEX 1404 double grating monochromator, a PMT, and lock-in amplifier (SR850) system, the output of which was recorded by the computer which also controlled the laser scan.

locity group within the Doppler profile of the pump transition as a significant simplification of the experimental conditions for the rest of the excitation scheme. This is achieved by keeping the pump laser fixed to the chosen frequency within the Doppler profile of the pump transition. Such experiments have enabled several interesting applications of coherence and quantum interference effects in molecular systems. These include molecular angular momentum alignment,[28] measurement of the electronic transition dipole moment between the ground state and the first excited state of a Doppler broadened molecular system,[29] and mapping of the internuclear distance dependence of the electronic transition dipole moment.[30] In addition, our recent experiments[31] confirm earlier predictions[32,33] that the AT effect can also be used to control valence electron spin polarization by modifying the mixing coefficients of a singlet-triplet pair of rovibrational levels perturbed by the spin-orbit interaction, an example of quantum control of the interaction of the quantum participants.

In our work earlier on mapping the absolute electronic transition dipole moment function of the $Na_2\ A\ ^1\Sigma_u^+ - X\ ^1\Sigma_g^+$ system[30] we have combined the *R*-centroid approximation with the AT splitting measurements. In contrast to intensity measurements and lifetime measurements, this method requires only an accurate measurement of the coupling laser electric field amplitude E and determination of the Rabi frequency Ω from an AT-split fluorescence spectrum. The AT splitting, which is proportional to the Rabi frequency $\Omega = \mu E/\hbar$, readily yields the electronic transition dipole matrix element μ. More recently it has been demonstrated that a combination of AT splitting measurements and fluorescence intensity measurements can be used to determine molecular transition dipole moment functions over a large range of internuclear separation R.[34] While the fluorescence intensity measurements yield many transition dipole moment matrix elements including ones for weak transitions, the measured values are only relative. When combining fluorescence and AT splitting measurements, the latter can be performed for a few of the strongest transitions and subsequently used to normalize the fluorescence-intensity-based measurements to an absolute scale, thus providing a test of theoretical calculations on an absolute basis even in cases when the molecular transitions are not strong.

In this paper we report the mapping of the electronic transition dipole moment internuclear distance dependence for the $^7Li_2\ A\ ^1\Sigma_u^+ - X\ ^1\Sigma_g^+$ system. The lithium dimer, the smallest molecule with core electrons, has a relatively simple electronic structure and thus presents an excellent system for developing and testing experimental and theoretical methods in laser spectroscopy. Compared to the $Na_2\ A\ ^1\Sigma_u^+ - X\ ^1\Sigma_g^+$ system,[30] we expect the agreement between experiment and theory to be better in the $^7Li_2\ A\ ^1\Sigma_u^+ - X\ ^1\Sigma_g^+$ case than in the $Na_2\ A\ ^1\Sigma_u^+ - X\ ^1\Sigma_g^+$ case.

For Li_2 theoretical information on the transition dipole moments between the ground and low-lying excited ungerade potentials was previously available from Refs. 35 and 36. The calculations were performed using model potential method[35] and multiconfiguration self-consistent-field approximation.[36] We are unaware of any other direct measurements of the $^7Li_2\ A\ ^1\Sigma_u^+ - X\ ^1\Sigma_g^+$ transition dipole moment.

For comparison with our Autler-Townes splitting based measurements, in this paper we present new *ab initio* theoretical calculations of the transition dipole moment for the $^7Li_2\ A\ ^1\Sigma_u^+ - X\ ^1\Sigma_g^+$ system that apply two different quantum-mechanical models: an all-electron valence bond self-consistent-field (VB-SCF)[37,38] method and a pseudopotential molecular orbital method.[39–42]

TABLE I. List of $F\ ^1\Sigma_g^+(v,J)$, $A\ ^1\Sigma_u^+(v',J')$, $X\ ^1\Sigma_g^+(v'',J'')$, and $X\ ^1\Sigma_g^+(v_1'',J_1'')$ state combinations used in our experiment to achieve OODR with corresponding laser wavenumbers. L_1 and L_2 laser wavenumbers were obtained from laser control software and corrected using a particular laser's calibration. The L_3 laser wavenumber was obtained from a Burleigh WA-1600 wavemeter after a resonance condition was achieved.

$F\ ^1\Sigma_g^+$ (v,J)	$A\ ^1\Sigma_u^+$ (v',J')	$X\ ^1\Sigma_g^+$ (v'',J'')	$X\ ^1\Sigma_g^+$ (v_1'',J_1'')	Pump laser L_1 (cm^{-1})	Probe laser L_2 (cm^{-1})	Coupling laser L_3 (cm^{-1})
16,11	17,10	2,11	17,11	17 184.637	15 137.928	12 735.897
16,11	17,10	2,11	19,11	17 184.637	15 137.928	12 252.877
16,11	17,10	2,11	21,9	17 184.637	15 137.928	11 819.989
16,11	17,10	2,11	22,9	17 184.637	15 137.928	11 604.729
16,11	17,10	2,11	24,9	17 184.637	15 137.928	11 199.515
17,11	18,10	2,9	18,9	17 389.229	15 102.344	12 712.124
17,11	18,10	2,9	20,9	17 389.229	15 102.344	12 221.992
17,11	18,10	2,9	23,9	17 389.229	15 102.344	11 578.071
17,11	18,10	2,9	25,11	17 389.229	15 102.344	11 191.732
18,11	19,10	2,11	26,11	17 558.281	15 067.953	11 208.849
18,11	19,10	2,11	26,9	17 558.281	15 067.953	11 226.225
20,11	21,10	3,11	25,9	17 304.373	15 001.114	11 789.818
20,11	21,10	3,11	25,11	17 304.373	15 001.114	11 771.712
20,11	21,10	3,11	27,9	17 304.373	15 001.114	11 439.843
20,11	21,10	3,11	27,11	17 304.373	15 001.114	11 423.341
20,11	21,10	3,11	28,9	17 304.373	15 001.114	11 280.722
20,11	21,10	3,11	28,11	17 304.373	15 001.114	11 264.613
21,11	22,10	4,11	26,9	17 464.561	14 969.484	11 797.013
21,11	22,10	4,11	26,11	17 464.561	14 969.484	11 779.521
21,11	22,10	4,11	28,11	17 464.561	14 969.484	11 451.605

II. EXPERIMENT

The four-level coherently driven extended Λ excitation scheme, illustrated in Fig. 1, and described in detail in Ref. 29, was used with two dye laser beams copropagating in the opposite direction of the coupling laser. The pump and probe lasers were Coherent Autoscan 699-29 dye lasers and the coupling laser was a Coherent 899-29 titanium sapphire laser, all with 0.5 MHz frequency bandwidth. The experimental setup is shown in Fig. 2. Lithium was heated in a five-arm heat pipe oven to about 700 °C. Argon gas was used as a buffer gas with a pressure of about 100–200 mTorr. A mechanical chopper was used to modulate one of the laser beams for phase-sensitive detection. The pump laser, operating with R6G dye, was used to excite population from thermally populated ground state levels to well known rovibrational levels in the $A\ ^1\Sigma_u^+$ state.[43] The probe laser operating with DCM dye moved population to the $F\ ^1\Sigma_g^+$ state[44,45] from the $A\ ^1\Sigma_u^+$ state. To calculate resonance frequencies and rovibronic wave functions, molecular constants from Ref. 46 were used for $^7Li_2\ X\ ^1\Sigma_g^+$ ground state. In these calculations the LEVEL 8.0 computer program was used to solve the radial Schrödinger equation.[47] The double resonance signal resulting from the probe laser scan was detected by a photomultiplier tube (PMT) and lock-in amplifier (SR850) system, the output of which was recorded by the computer used to control the laser scan. Neutral density filters were used to control the power of the lasers. A third laser, the titanium sapphire laser, was used as the coupling laser between the ground $X\ ^1\Sigma_g^+$ state and the $A\ ^1\Sigma_u^+$ state. This laser had a higher power than the pump and probe dye lasers. The former was fixed to a resonance frequency corresponding to a selected velocity group within the Doppler profile of ground state molecules. The latter was used to observe the AT splitting by monitoring fluorescence resulting from the scan of this laser through the probe transition. This fluorescence was detected by monitoring a spectrally isolated fluorescence transition from the excited state by using the SPEX 1404 double monochromator as a narrow band filter. Initially the three laser beams were carefully overlapped by maximizing the optical-optical double resonance (OODR) fluorescence signal. For finer adjustment of the overlap, the magnitude of the observed AT splitting was used to maximize the overlap. The desirable spot size for each laser was obtained with a lens or a combination of two lenses. The spot size of the laser was measured by using a razor blade technique with an accuracy of 10 μm.[48] In order to ensure E field homogeneity of the coupling field in the interaction region of the three laser beams, the spot size of the coupling laser was kept about twice as large as the probe and pump laser spot sizes. In the experiment, typical laser powers were about 3, 20, and >200 mW for the pump laser (L_1), probe laser (L_2), and coupling laser (L_3), respectively. The power of laser beams was measured with coherent Lasermate/D power meter with an absolute accuracy of 1.5%.

III. RESULTS AND DISCUSSION

The AT splitting spectra were observed by monitoring $F\ ^1\Sigma_g^+(v,J)-A\ ^1\Sigma_u^+(v_1',J_1')$ fluorescence as a function of the probe laser L_2 detuning around the resonance frequency of the $F\ ^1\Sigma_g^+(v,J)-A\ ^1\Sigma_u^+(v',J')$ transition, while the pump laser L_1 was held fixed at the resonance frequency of the $A\ ^1\Sigma_u^+(v',J')-X\ ^1\Sigma_g^+(v'',J'')$ transition. Table I lists the combinations of rovibronic energy levels used in our experiment. Different background colors distinguish the various OODR

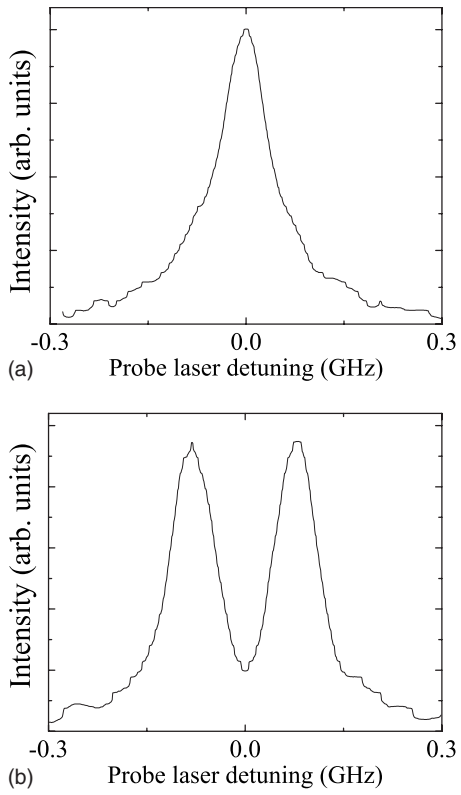

FIG. 3. Spectra observed monitoring $F\ ^1\Sigma_g^+(v=16,J=11)-A\ ^1\Sigma_u^+(v'=8,J'=10)$ fluorescence as a function of the detuning of the probe laser. (a) OODR spectrum observed without the coupling laser L_3 when the pump laser L_1 was held fixed at the $A\ ^1\Sigma_u^+(v'=17,J'=10)-X\ ^1\Sigma_g^+(v''=2,J''=9)$ resonance frequency and the probe laser L_2 was modulated and scanned. The laser power values of lasers L_1 and L_2 were 23 and 2.4 mW, respectively. (b) The AT-split spectrum was observed when the coupling $(A\ ^1\Sigma_u^+(v'=17,J'=10)-X\ ^1\Sigma_g^+(v''=17,J''=11))$ and pump lasers L_3 and L_1 were held fixed on resonance and the probe laser L_2 was modulated and scanned. The laser power values of L_1, L_2, and L_3 were 23, 2.4, and 498 mW, respectively.

conditions used in this experiment. Pump and probe laser wavenumbers were calibrated using the standard Doppler-limited iodine calibration.[49] The coupling laser wavenumber was monitored by a Burleigh WA-1600 wavemeter when the coupling laser was held at the resonance frequency.

The resulting OODR signal is illustrated in Fig. 3(a). The probe laser scan is shown for the excitation sequence $F\ ^1\Sigma_g^+(v=16,J=11)-A\ ^1\Sigma_u^+(v'=17,J'=10)-X\ ^1\Sigma_g^+(v''=2,J''=9)$ followed by fluorescence decay to the $A\ ^1\Sigma_u^+(v'=8,J'=10)$ level. When the coupling laser L_3 beam was added to this excitation scheme, it was held fixed at resonance frequency of another $A\ ^1\Sigma_u^+(v',J')-X\ ^1\Sigma_g^+(v_1'',J_1'')$ transition with a larger Franck–Condon factor to enhance its Rabi frequency. A subsequent probe laser scan produced the desired AT splitting, as is illustrated in Fig. 3(b). The coupling laser was held fixed to the $A\ ^1\Sigma_u^+(v'=17,J'=10)-X\ ^1\Sigma_g^+(v''=17,J''=11)$ transition resonance frequency. All other coupling laser transitions used in this work are listed in Table II. The spot sizes and powers of L_1, L_2, and L_3 were 400, 240, and 540 μm and 23, 2.4, and 498 mW, respectively. The pump and probe laser powers were kept as low as possible to have a minimal effect on the observed AT splitting spectrum and yet result in an acceptable signal to noise ratio. To test the effect of the coupling laser L_3 power on the AT splitting signal, the pump and probe laser powers were kept constant while the coupling laser power was varied between 100 and 500 mW, as shown in Fig. 4. The experiment indicates a linear dependence between the experimentally observed AT splitting and the coupling laser Rabi frequency, which is linearly proportional to the square root of the coupling laser power.

The AT splitting spectra were used to calculate the electronic transition dipole moment matrix element for the $A\ ^1\Sigma_u^+(v',J')-X\ ^1\Sigma_g^+(v'',J'')$ transition of $^7Li_2$. Density ma-

TABLE II. List of experimentally determined transition dipole moment matrix elements μ_{expt} and their R-centroid values for the $A\ ^1\Sigma_u^+-X\ ^1\Sigma_g^+$ system.

v'	J'	v_1''	J_1''	μ_{expt} (D)	R_{centroid} (Å)	$\mu_e(R_c)$ (D)	$\langle v'J'\vert v''J''\rangle$
17	10	17	11	1.58	3.24	9.0788	0.174 15
17	10	19	11	1.87	3.39	9.3314	−0.200 69
17	10	21	9	1.81	3.55	9.5896	0.188 51
17	10	22	9	1.52	3.61	9.7776	−0.154 98
17	10	24	9	5.17	4.40	10.0285	0.515 82
18	10	18	9	1.19	3.28	9.1229	0.129 95
18	10	20	9	1.82	3.41	9.3570	−0.194 25
18	10	23	9	1.28	3.47	9.7888	−0.130 8
18	10	25	11	5.90	4.46	10.0209	0.588 81
21	10	25	9	1.98	3.81	9.6205	0.205 71
21	10	25	11	1.94	3.83	9.6203	0.202 01
21	10	27	9	2.49	5.45	9.8928	0.251 23
21	10	27	11	2.79	5.31	9.8983	0.282 01
21	10	28	9	6.31	4.59	9.9753	0.632 91
21	10	28	11	6.21	4.59	9.9782	0.622 69
19	10	26	9	6.24	4.51	10.0093	0.623 32
19	10	26	11	6.36	4.54	10.0138	0.635 49
22	10	26	9	2.10	3.98	9.6426	0.217 65
22	10	26	11	2.07	4.01	9.6440	0.214 99
22	10	28	11	3.81	5.14	9.8741	0.385 53

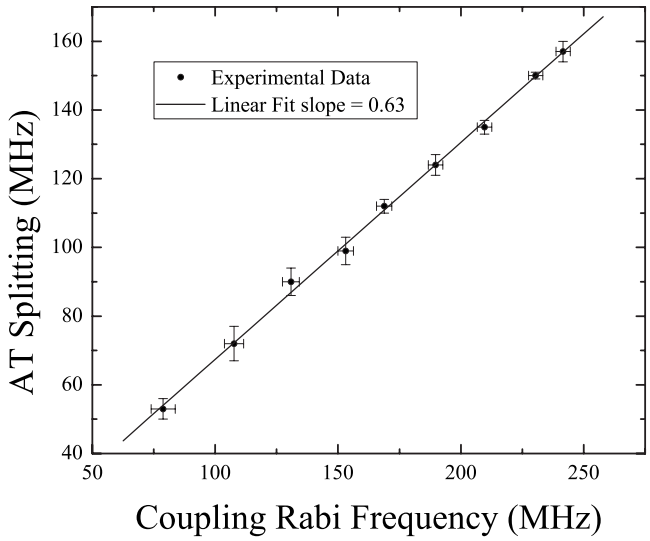

FIG. 4. AT splitting vs coupling laser Rabi frequency: the probe laser scan for the excitation sequence $F\ ^1\Sigma_g^+(v=16,J=11)\leftarrow A\ ^1\Sigma_u^+(v'=17,J'=10)\leftarrow X\ ^1\Sigma_g^+(v''=2,J''=9)$ was detected by monitoring fluorescence decay to the $A\ ^1\Sigma_u^+(v'=8,J'=10)$ level while the coupling laser L_3 was held fixed at the resonance frequency of the $A\ ^1\Sigma_u^+(v'=17,J'=10)\leftarrow X\ ^1\Sigma_g^+(v''=17,J''=11)$ transition. The power of the coupling laser was varied between 100 and 500 mW to monitor the coupling laser power dependence of the AT splitting.

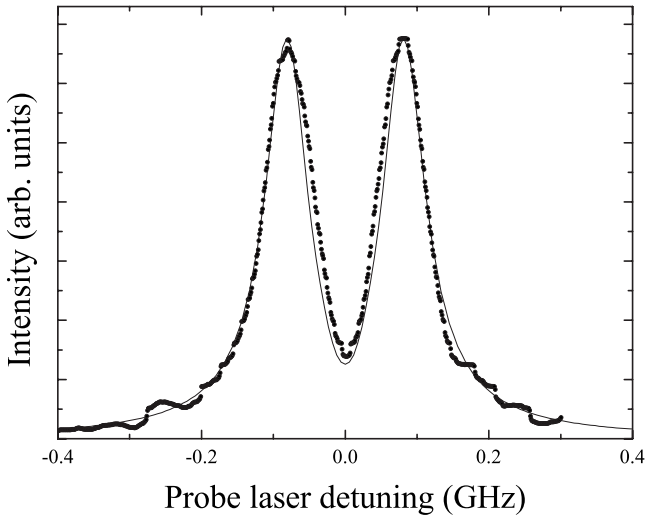

FIG. 5. The solid line shows the experimental AT splitting with the coupling laser on resonance with the $A\ ^1\Sigma_u^+(v'=17,J'=10)\leftarrow X\ ^1\Sigma_g^+(v''=17,J''=11)$ transition. The dashed line shows density matrix equations-of-motion-based simulation. The branching ratios were $W_{32}/W_3=0.06$, $W_{21}/W_2=0.005$, and $W_{24}/W_2=0.04$; the Doppler width was 2.9 GHz; the transit relaxation rate was $w_1/2\pi=5$ MHz; the Rabi frequencies were $\Omega_{21}/2\pi=9.08$ MHz and $\Omega_{32}/2\pi=58.22$ MHz; and the Rabi frequency of the coupling field $\Omega_{24}=241.62$ MHz was obtained from a best fit to the recorded experimental spectrum. Using the expression for the Rabi frequency $\Omega_{24}=\mu E/\hbar$, the transition dipole moment matrix element $\mu=1.57\pm0.1$ D is determined for $A\ ^1\Sigma_u^+(v'=17,J'=10)\leftarrow X\ ^1\Sigma_g^+(v''=17,J''=11)$ transition.

trix equations-of-motion-based simulations were used for this purpose, as described in Ref. 29, to fit the experimental AT splitting spectra by varying the Rabi frequency of the coupling field Ω_{24}. After obtaining Ω_{24} from the best fit we used the expression $\Omega_{24}=\mu E/\hbar$ to calculate the transition dipole moment matrix element μ between the rovibrational levels coupled by E_3. Here μ is the transition dipole moment matrix element and E is the coupling laser electric field defined by

$$E=\sqrt{\frac{2}{c\varepsilon_0}}\cdot\sqrt{\frac{2P_{\mathrm{tot}}}{\pi w^2}}.$$

In this expression P_{tot} is the measured laser power and w is the spot size radius at which the intensity is reduced from its maximum value by a factor of $1/e^2$. The observed and simulated spectra are shown for comparison in Fig. 5. In this case the probe laser scan for the excitation sequence $F\ ^1\Sigma_g^+(v=16,J=11)-A\ ^1\Sigma_u^+(v'=17,J'=10)-X\ ^1\Sigma_g^+(v''=2,J''=9)$ is followed by fluorescence decay to the $A\ ^1\Sigma_u^+(v'=8,J'=10)$ level when the coupling laser L_3 was held fixed at the resonance frequency of the $A\ ^1\Sigma_u^+(v'=17,J'=10)-X\ ^1\Sigma_g^+(v''=17,J''=11)$ transition. In the simulation illustrated with a solid line in Fig. 5, the following parameter values were used. The laser spot sizes[48] and powers for L_1, L_2, and L_3 were 402, 238, and 536 μm and 23, 2.4, and 498 mW, respectively. Lifetimes of the $A\ ^1\Sigma_u^+(v'=8,J'=10)$ and the $F\ ^1\Sigma_g^+(v=16,J=11)$ levels were $\tau_2=18.63$ ns (Ref. 50) and $\tau_3=8.47$ ns (calculated value), respectively. The branching ratios were $W_{32}/W_3=0.06$, $W_{21}/W_2=0.005$, and $W_{24}/W_2=0.04$. W_{ij}/W_i represents the fraction of population decaying from level i to level j. The Doppler width was 2.9 GHz. The transit relaxation rate $w_1/2\pi=5.0$ MHz was calculated according to Sagle *et al.*[51] The pump and the probe laser Rabi frequencies were $\Omega_{21}/2\pi=9.08$ MHz and $\Omega_{32}/2\pi=58.22$ MHz based on the experimental laser power values in the interaction region. The Rabi frequency of the coupling field $\Omega_{24}/2\pi=241.62$ MHz was then obtained from best fit to the recorded experimental spectrum. Using the expression $\Omega_{24}=\mu E/\hbar$, the resulting transition dipole moment matrix element is $\mu=1.57\pm0.1$ D for the $A\ ^1\Sigma_u^+(v'=17,J'=10)-X\ ^1\Sigma_g^+(v''=17,J''=11)$ transition.

The transition dipole matrix element is defined as $\mu=\langle v'J'|\mu_e(R)|v''J''\rangle$, which represents an overlap integral of the wave functions of the two levels weighted with the electronic transition dipole moment $\mu_e(R)$. Table II shows the list of the $\mu_e(R)$ calculated from experimentally measured transition dipole matrix elements for the $A\ ^1\Sigma_u^+-X\ ^1\Sigma_g^+$ rovibrational transitions as a function of the R-centroid values for R.[52] For each data point the AT-split line profile was observed at least five times to estimate the experimental error. Using these experimental results for each data point we calculated a mean value of the AT splitting and the standard deviation to describe the experimental error. The other error sources were the error in the measurement of the laser power and the coupling laser spot size. Reasonable estimates for these parameters were 5 mW and 10 μm, respectively.

To compare our experimental results with theory, we have calculated $\mu_e(R)$ between the $A\ ^1\Sigma_u^+-X\ ^1\Sigma_g^+$ states by a valence bond as well as a pseudopotential method to be discussed below. Subsequently the LEVEL 8.0 program[47] was used to calculate theoretical transition dipole moment matrix elements using the two *ab initio* theoretical transition dipole moment $\mu_e(R)$ functions. The difference between the experimental and theoretical transition dipole moment matrix elements is shown in Fig. 6 as a function of the calculated

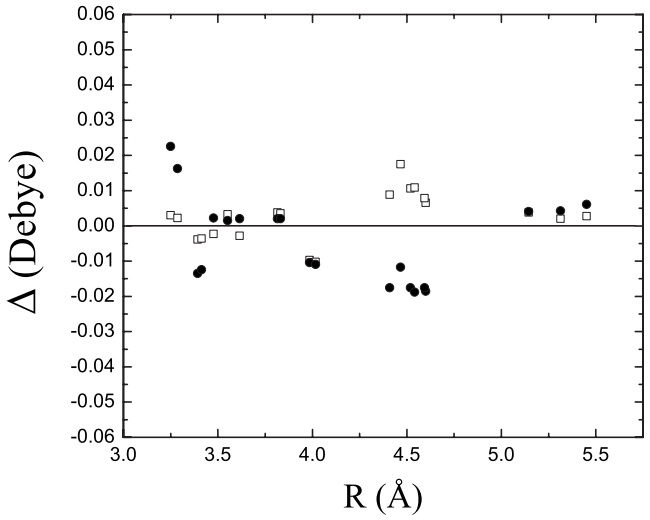

FIG. 6. The difference (Δ) between experimental and theoretical transition dipole moment matrix elements vs the calculated *R*-centroid value for each transition. The dots and the squares denote the difference between the experimental and calculated values for the VB-SCF method and the pseudopotential molecular orbital method, respectively. The difference Δ is very small (~1%) in comparison with the values of the transition dipole moment matrix elements, which are given in Table II.

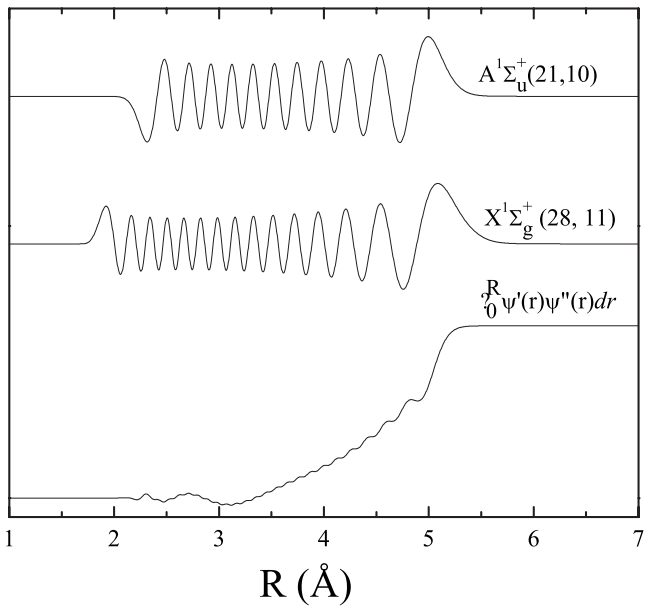

FIG. 7. Plot of the excited state $A\ ^1\Sigma_u^+(v',J')$ and ground state $X\ ^1\Sigma_g^+(v'',J'')$ wave functions ψ' and ψ'' as a function of internuclear distance R and the overlap integral $\int_0^R \Psi'(r)\Psi''(r)dr$ for the $A\ ^1\Sigma_u^+(21,10)$ and $X\ ^1\Sigma_g^+(28,11)$ rovibrational levels.

R-centroid value. The dots denote the difference between experiment and theory using the VB-SCF method based $\mu_e(R)$ function and the squares show the same for the $\mu_e(R)$ function calculated using the pseudopotential molecular orbital method.

The *R*-centroid method can be used in cases where there is only one stationary phase point in the overlap integral and the integral accumulates over a small *R* interval. When there is more than one stationary phase point and the integral accumulates over a relatively large *R* interval, the *R*-centroid approximation cannot be used reliably. In such cases a higher order polynomial expansion has to be used for representing the electronic transition dipole moment function $\mu_e(R)$. We have calculated the overlap integrals

$$\int_0^R \Psi'(r)\Psi''(r)dr$$

for all coupling transitions we have used in order to be able to understand how well the *R*-centroid approximation[52,53] applies in each case. In Fig. 7 we have plotted as an example the accumulation of the overlap integral as a function of *R* for one of the coupling transitions used. One can easily see that the integral accumulates over a relatively large *R* range. Similar behavior of the overlap integral was observed for almost all of our coupling transitions. Thus for obtaining $\mu_e(R)$ from the experimentally measured transition dipole moments μ given in Table II we have used the following polynomial expansion of the electronic transition dipole moment:

$$\mu_e(R) = \mu_0 + \mu_1 R + \mu_2 R^2.$$

We have limited the expansion to second order since the inclusion of higher order terms did not improve substantially the fit for $\mu_e(R)$. From the fitting procedure we obtained the following coefficient values: μ_0=0.064 D, μ_1=4.43 D/Å, and μ_2=−0.49 D/Å^2. Figure 8 shows comparison between quadratic polynomial expansion fit (solid line) and the *ab initio* calculation (pseudopotential MO—dashed line) provided by Magnier and the *ab initio* calculation (VB-SCF—dotted line) provided by Kotochigova. As indicated in Figs. 6 and 8, our experimental results are in very good agreement with theoretical calculations (Table III).

IV. THEORETICAL CALCULATIONS

A. VB-SCF method

The VB-SCF method is an all-electron calculation, in which all six electrons of Li_2 are in the active space and

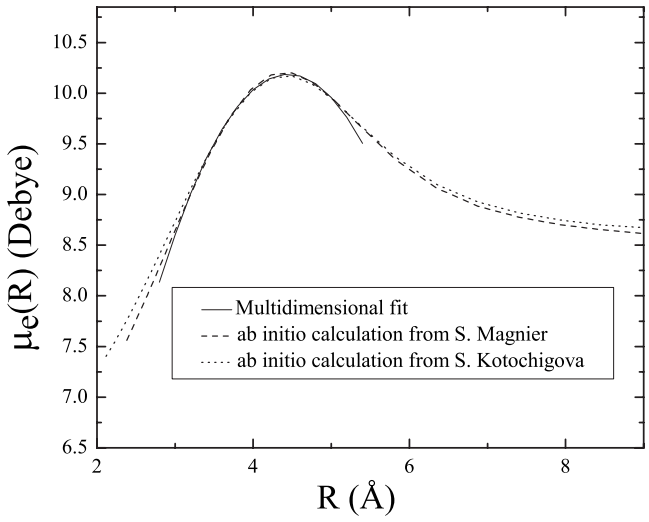

FIG. 8. Comparison between the experimental and theoretical transition dipole moments. The results from the fit of experimental transition dipole moment matrix elements with a quadratic polynomial expansion are given as a solid line.

TABLE III. Calculated *ab initio* transition dipole moments. The first two columns list theoretical calculations done by Magnier using the pseudopotential molecular orbital method. The last two columns list theoretical calculation done by Kotochigova using the VB-SCF method.

Pseudopotential molecular orbital method		VB-SCF method	
R (a.u.)	$\mu_e(R)$ (D)	R (a.u.)	$\mu_e(R)$ (D)
4.5	7.562	4.0	7.402
5.0	8.007	4.2	7.537
5.5	8.484	4.4	7.682
6.0	8.960	4.6	7.834
6.5	9.399	4.8	7.994
7.0	9.768	5.0	8.159
7.5	10.037	5.2	8.328
8.0	10.182	5.4	8.501
8.5	10.200	5.6	8.672
9.0	10.106	5.8	8.844
9.5	9.938	6.0	9.014
10.0	9.735	6.2	9.179
11.0	9.343	6.4	9.337
12.0	9.061	6.6	9.487
13.0	8.883	6.8	9.627
14.0	8.774	7.0	9.755
15.0	8.700	7.5	10.007
16.0	8.652	8.0	10.148
17.0	8.614	8.5	10.170
18.0	8.589	9.0	10.087
19.0	8.566	9.5	9.932
20.0	8.550	10.0	9.741
22.0	8.525	11.0	9.370
24.0	8.510	12.0	9.099
26.0	8.497	13.0	8.927
28.0	8.489	14.0	8.818
30.0	8.482	15.0	8.747
32.0	8.479	16.0	8.698
34.0	8.474	20.0	8.600
38.0	8.469		
40.0	8.467		

contribute to the bonding. For large internuclear separations the valence bond molecular wave function becomes a product of atomic electronic wave functions, and thus the molecule dissociates correctly. Atomic Hartree–Fock functions describe the occupied $1s^2$, $2s$, and $2p$ single-electron orbitals of the constituent Li atoms while Sturm functions serve as a basis set for unoccupied orbitals. These single-electron Hartree–Fock functions are obtained by solving the integrodifferential Hartree–Fock equations self-consistently. Single-electron Sturm orbitals are obtained by solving the Hartree–Fock–Sturm equations.[37]

In order to obtain accurate molecular properties, highly correlated electronic wave functions are necessary. We use the VB-SCF wave functions as a zeroth-order approximation for an extended configuration interaction (CI) calculation. In the CI method we include all single, double, and triple excitations relative to the $1s^22s+1s^22s$ and $1s^22s+1s^22p$ reference configurations for the ground and excited states, respectively. The CI coefficients are determined variationally. The CI wave functions are used to calculate the electronic transition dipole moments between the $X\ ^1\Sigma_g^+(\Omega=0^+)$ state and the excited $A\ ^1\Sigma_u^+(\Omega=0^+)$ state dissociating to the $1s^22s+1s^22p$ limit. The VB-SCF transition dipole moment as a function of internuclear separation is shown in Fig. 8. For large R (not shown in the figure) the transition dipole moment becomes independent of R and is determined by the Li $2s-2p(^2P_{1/2})$ transition dipole moment. We estimate the uncertainty of the theoretical transition dipole moment as 0.2 D based on a comparison of the dipole moment at $R=100a_0$ with the experimental dipole moment of the Li atom.[54]

B. Pseudopotential molecular orbital method

In the pseudopotential method the Li_2 molecule is treated as a two valence electron system in which the two electrons move in the field of the ionic frozen cores Li^+. In this approach, interactions are represented by effective potentials. Interactions among the two electrons and the two Li^+ cores are described by the one-electron pseudopotential determined by Durant and Barthelat[39] while core-polarization effects are taken into account through a core-polarization potential.[42] Electronic correlation for the two valence electrons is considered through full CI calculations.

The pseudopotential method is currently used in the description of the electronic structure of alkali dimers and is well suited both for the lowest states and for highly excited states.[39–41] A contracted Gaussian basis set is used in the present work and consists of $9s$, $7p$, $5d$, and $1f$. Very diffuse orbitals have been introduced in order to describe accurately the lithium atom up to Li($5s$) (i.e., the ten first atomic levels). For example, in the case of the two lowest atomic states Li($2s$) and Li($2p$), the differences between experimental and calculated atomic energies are found to be 0.48 and 0.19 cm^{-1}, respectively. For the first 11 molecular dissociation limits [i.e., from Li($2s$)+Li($2s$) up to Li($2s$)+Li($5s$)], the average value of the difference between computed and experimental energies is found to be ~ 12 cm^{-1}. Potential energy curves and relevant dipole moments have been determined over a large range of R for all $^{1,3}\Lambda_{g,u}^{(+/-)}$ molecular states dissociating adiabatically up to the asymptote Li($2s$)+Li($2s$) and above, up to the asymptote Li($2s$)+Li($5s$) (i.e., for 86 molecular states).[55] Comparison with previous calculations[41] and available experimental data[42] is seen to be satisfying and, in particular, the description of highly excited states [correlated with asymptotes close to the Li($2p$)+Li($2p$) asymptote and below] has been improved. For the transition dipole moment, we obtain $\mu=5.98$ D for the transition $A\ ^1\Sigma_u^+-X\ ^1\Sigma_g^+$ at large distance, which is in good agreement with the atomic value[54] and with previous *ab initio* calculations [5.97(5) D (Ref. 56) and 5.966 D (Ref. 57)].

As shown in Fig. 8 the VB-SCF and the pseudopotential dipole moments are in excellent agreement. For the shortest R a small deviation is apparent. This is partly due to the different way in which interactions are included in the model for the two methods and also due to basis sets.

V. CONCLUSIONS

We have presented a comparison between experimental and theoretical electronic transition dipole moment values for the $^7Li_2$ $A\ ^1\Sigma_u^+ - X\ ^1\Sigma_g^+$ system. The experimental results, based on measuring the absolute magnitude of the transition dipole matrix elements for rovibronic transitions corresponding to different R-centroid values, are in excellent agreement with *ab initio* theoretical calculations of the transition dipole moment. Two different quantum-mechanical models were used for this comparison: an all-electron VB-SCF method and a pseudopotential molecular orbital method. As expected the agreement between experiment and theory is very good in this case since the $^7Li_2$ molecule is the smallest molecule with core electrons and as a result has a relatively simple electronic structure.

ACKNOWLEDGMENTS

This work was supported by the National Science Foundation Award No. PHY 0555608.

[1] S. E. Harris, Phys. Today **50** (7), 36 (1997).
[2] M. Fleischhauer and M. D. Lukin, Phys. Rev. Lett. **84**, 5094 (2000).
[3] S. A. Hopkins, E. Usadi, H. X. Chen, and A. V. Durant, Opt. Commun. **138**, 185 (1997).
[4] N. E. Karapanagioti, O. Faucher, Y. L. Shao, D. Charalambidis, H. Bachau, and E. Cormier, Phys. Rev. Lett. **74**, 2431 (1995).
[5] E. Arimondo, in *Progress in Optics XXXV*, edited by E. Wolf (North-Holland, Amsterdam, 1996).
[6] H. Y. Ling, Y. Q. Li, and M. Xiao, Phys. Rev. A **53**, 1014 (1996).
[7] O. Schmidt, R. Wynands, Z. Hussein, and D. Meschede, Phys. Rev. A **53**, R27 (1996).
[8] L. Hau, S. E. Harris, Z. Dutton, and C. H. Behroozi, Nature (London) **397**, 594 (1999).
[9] M. M. Kash, V. A. Sautenkov, A. S. Zibrov, L. Hollberg, G. R. Welch, M. D. Lukin, Y. Rostovtsev, E. S. Fry, and M. O. Scully, Phys. Rev. Lett. **82**, 5229 (1999).
[10] D. Budker, D. F. Kimball, S. M. Rochester, and V. V. Yashchuck, Phys. Rev. Lett. **83**, 1767 (1999).
[11] M. D. Lukin, A. B. Matsko, M. Fleischhauer, and M. O. Scully, Phys. Rev. Lett. **82**, 1847 (1999).
[12] F. C. Spano, J. Chem. Phys. **114**, 276 (2001).
[13] F. Renzoni, A. Lindner, and E. Arimondo, Phys. Rev. A **60**, 450 (1999).
[14] A. Imamoglu and S. E. Harris, Opt. Lett. **14**, 1344 (1989).
[15] K. J. Boller, A. Imamoglu, and S. E. Harris, Phys. Rev. Lett. **66**, 2593 (1991).
[16] See, for example, J. Gea-Banacloche, Y.-Q. Li, S.-Z. Jin, and M. Xiao, Phys. Rev. A **51**, 576 (1995).
[17] D. J. Fulton, S. Sheperd, R. R. Moseley, B. D. Sinclair, and M. H. Dunn, Phys. Rev. A **52**, 2302 (1995).
[18] M. A. Quesada, A. M. F. Lau, D. H. Parker, and D. W. Chandler, Phys. Rev. A **36**, 4107 (1987).
[19] J. Qi and A. M. Lyyra, Phys. Rev. A **73**, 043810 (2006).
[20] A. Lazoudis, E. H. Ahmed, L. Li, T. Kirova, P. Qi, A. Hansson, J. Magnes, and A. M. Lyyra, Phys. Rev. A **78**, 043405 (2008).
[21] E. Ahmed and A. M. Lyyra, Phys. Rev. A **76**, 053407 (2007).
[22] J. Qi, F. C. Spano, T. Kirova, A. Lazoudis, J. Magnes, L. Li, L. M. Narducci, R. W. Field, and A. M. Lyyra, Phys. Rev. Lett. **88**, 173003 (2002).
[23] R. Garcia-Fernandez, A. Ekers, J. Klavins, L. P. Yatsenko, N. B. Nikolai, B. W. Shore, and K. Bergmann, Phys. Rev. A **71**, 023401 (2005).
[24] A. Lazoudis, Ph.D. thesis, Temple University, 2005.
[25] A. M. Lyyra, H. Wang, T.-J. Whang, L. Li, and W. C. Stwalley, Phys. Rev. Lett. **66**, 2724 (1991).
[26] E. H. Ahmed, P. Qi, and A. M. Lyyra, "CW all-optical quadruple resonance spectroscopy; a coherently driven five level molecular system" (to be published).
[27] E. H. Ahmed, Ph.D. thesis, Temple University, 2007.
[28] J. Qi, G. Lazarov, X. Wang, L. Li, M. Narducci, A. M. Lyyra, and F. C. Spano, Phys. Rev. Lett. **83**, 288 (1999).
[29] E. Ahmed, A. Hansson, P. Qi, L. Li, T. Kirova, J. Qi, A. Lazoudis, S. Magnier, S. Kotochigova, and A. M. Lyyra, J. Chem. Phys. **124**, 084308 (2006).
[30] E. H. Ahmed, P. Qi, B. Beser, J. Bai, R. W. Field, J. P. Huennekens, and A. M. Lyyra, Phys. Rev. A **77**, 053414 (2008).
[31] O. Salihoglu, P. Qi, E. H. Ahmed, and A. M. Lyyra, "Quantum control of singlet-triplet character of molecular eigenstates" (to be published).
[32] T. Kirova, Ph.D. thesis, Temple University, 2005.
[33] T. Kirova and F. Spano, Phys. Rev. A **71**, 063816 (2005).
[34] S. J. Sweeney, E. H. Ahmed, P. Qi, A. M. Lyyra, and J. Huennekens, J. Chem. Phys. **129**, 154303 (2008).
[35] D. K. Watson, Chem. Phys. Lett. **51**, 513 (1977).
[36] D. D. Konowalow, M. E. Rosenkrantz, and D. S. Hochhauser, J. Mol. Spectrosc. **99**, 321 (1983).
[37] S. Kotochigova, J. Chem. Phys. **128**, 024303 (2008).
[38] S. Kotochigova and E. Tiesinga, J. Chem. Phys. **123**, 174304 (2005).
[39] P. Durant and J. C. Barthelat, Theor. Chim. Acta **38**, 283 (1975).
[40] M. Foucrault, P. Millié, and J. P. Daudey, J. Chem. Phys. **96**, 1257 (1992).
[41] R. Poteau and F. Spiegelmann, J. Mol. Spectrosc. **171**, 299 (1995).
[42] S. Magnier, M. Aubert-Frécon, and A. R. Allouche, J. Chem. Phys. **121**, 1771 (2004).
[43] K. Urbanski, S. Antonova, A. Yiannopoulou, A. M. Lyyra, and W. C. Stwalley, J. Chem. Phys. **104**, 2813 (1996); **116**, 10557(E) (2002).
[44] S. Antonova, G. Lazarov, K. Urbanski, A. M. Lyyra, L. Li, G.-H. Jeung, and W. C. Stwalley, J. Chem. Phys. **112**, 7080 (2000).
[45] P. Qi, G. Lazarov, and A. M. Lyyra, J. Mol. Spectrosc. **247**, 184 (2008).
[46] P. Kusch and M. M. Hessel, J. Chem. Phys. **67**, 586 (1977).
[47] R. J. Le Roy, "LEVEL 8.0: Computer program for solving the radial Schrodinger equation for bound and quasibound levels," Chemical Physics Research Report No. CP-663, University of Waterloo, 2007.
[48] D. R. Skinner and R. E. Whitcher, J. Phys. E **5**, 237 (1972).
[49] The Aimé Cotton Iodine Atlas, S. Gerstenkorn and P. Luc, Atlas du Spectre d'Absorption de la Molecule d'Iode, Editions du CNRS, Paris, 1978, was recalibrated in S. Gerstenkorn and P. Luc, Rev. Phys. Appl. **14**, 791 (1979).
[50] G. Baumgartner, H. Kornmeier, and W. Preuss, Chem. Phys. Lett. **107**, 13 (1984).
[51] J. Sagle, R. K. Namiotka, and J. Huennekens, J. Phys. B **29**, 2629 (1996).
[52] C. Noda and R. N. Zare, J. Mol. Spectrosc. **95**, 254 (1982).
[53] S. M. Yazykova and E. V. Butyrskaya, J. Phys. B **13**, 3361 (1980).
[54] W. I. McAlexander, E. R. I. Abraham, and R. G. Hulet, Phys. Rev. A **54**, R5 (1996).
[55] S. Magnier, "Lithium dimer potential energy curves and dipole moments up to the Li(2*s*) + Li(5*s*) asymptote" (to be published).
[56] D. D. Konowalow and J. L. Fish, Chem. Phys. **84**, 463 (1984).
[57] I. Schmidt-Mink, W. Müller, and W. Meyer, Chem. Phys. **92**, 263 (1985).